Magnetic Anisotropy of Cerium Endohedral Metallofullerenes

Masayasu Inakuma,*,† Haruhito Kato,‡ Atsushi Taninaka,‡ Hisanori Shinohara,‡ and Toshiaki Enoki*,†

Department of Chemistry, Tokyo Institute of Technology, Tokyo 152-8551, Japan, and Department of Chemistry, Nagoya University, Nagoya 464-8602, Japan

Received: November 26, 2002; In Final Form: May 23, 2003

Cerium endohedral metallofullerene ($Ce@C_{82}$) is a π−f composite nanomagnet, where anisotropic f-electron spin is expected to couple with the rotational motion of the fullerene cage that has π-electron spin. The field cooling effect on the susceptibility of $Ce@C_{82}$ in organic solutions suggests that the application of a magnetic field forces the molecular orientations to be aligned, in cooperation with the magnetic anisotropy of the f-electron spin coupled with the molecular orientation. The role of crystal field in the magnetic anisotropy, which is associated with the off-center geometry of the Ce ion in the cage, is clarified by the crystal field analysis. The crystal field effect in the metallofullerene cage is considerably reduced, in contrast to that of ordinary rare-earth compounds. This is consistent with the findings of a small electronic coupling between the f and π electrons and a shallow potential of the surrounding cage to the Ce ion. As a consequence, the crystal field effect is emphasized in the low-temperature range (below ∼100 K).

1. Introduction

Many of the rare-earth elements are encapsulated in a fullerene cage, giving endohedral metallofullerenes.[1] The electronic structure of the mono metallofullerenes consists of an interior metal cation and the exterior π electrons on the cage, where the charge transfer from the encapsulated metal atom generates a complex state $M^{n+}@C_x^{n-}$ (where M is a rare-earth metal, x is the number of C atoms, and n is the valence).[2−4] From a magnetism aspect, rare-earth-including endohedral metallofullerenes are of particular interest, because the interplay between the f-electron spins of the rare-earth atom and the π-electron spins of the cage is expected to produce unconventional magnetic features. Considering the structure of endohedral mono metallofullerenes such as $Sc@C_{82}$, $Y@C_{82}$, and $La@C_{82}$,[5−8] the interior crystal field that acts on the encapsulated metal ion could be assumed to be anisotropic, because the metal ion is located off-center of the spherical cage. Therefore, the rare-earth f-electron spin is subjected to a magnetic anisotropy, because of the ion within the crystal field of the cage, where the π-electron spin is delocalized. Thus, the metallofullerenes are characterized as anisotropic hybrid nanomagnets. In the meantime, the spherical-shaped fullerene cage can be rotated with low rotational energy, even in the solid state. The magnetism of the nanomagnet, coupled with its motion or direction, is an attractive subject, because the magnetism of the anisotropic nanomagnets can be controlled by rotating the molecules and vice versa.

The magnetism of the endohedral rare-earth metallofullerenes, such as $La@C_{82}$,[9,10] $Ce@C_{82}$,[10−12] $Gd@C_{82}$,[9,13−15] and $M@C_{82}$ (where M = Tb, Dy, Ho, and Er),[14,15] has been studied, in relation to the crystal structures, where the magnetic moments are treated as spins in free rare-earth ions. However, the simple free spin model has not given a full account of both the magnetic properties and the electronic structure of the metallofullerenes, including the π-electron spin on the cage. Previous studies have involved the crystal field effect for improving the free spin model, with an explanation of the deviant magnetic behaviors of metallofullerenes.[11,12,14,15] The crystal field effect in the metallofullerene cage, however, has not been investigated quantitatively. The structure of the mono metallofullerene $M@C_{82}$ most abundantly produced—the so-called isomer I or A—has C_{2v} symmetry.[5,7,16] The major isomers of $Ce@C_{82}$, $La@C_{82}$, and $Gd@C_{82}$ are considered to have their respective ions with the same trivalence in the cage with the same symmetry.[17] On one hand, the difference between the respective trivalent ions in $Ce@C_{82}$ and $La@C_{82}$ is the existence of the 4f electron in the former. On the other hand, the difference between the respective trivalent ions in $Ce@C_{82}$ and $Gd@C_{82}$ is the existence (or absence) of the orbital angular momentum: $L = 3$ and $L = 0$, respectively. The cooperation of the orbital angular momentum and the low-symmetry crystal electric field can induce anisotropic magnetism in $Ce@C_{82}$. Comparing the magnetic behavior of these three metallofullerenes can reveal the crystal field effect on the interior Ce^{3+} ions in $Ce@C_{82}$.

In the present study, we have measured the temperature-dependent magnetic susceptibility and the isothermal magnetization of the solutions ($Ce@C_{82}$, $Gd@C_{82}$) with organic solvents and the solid films ($Ce@C_{82}$, $La@C_{82}$). Through comparison of the magnetic behavior of these two sets of metallofullerenes, we discuss the magnetism and the crystal field effect of the metallofullerenes. The magnetic susceptibility of the solution samples revealed the correlation of the motion with the anisotropic magnetism of $Ce@C_{82}$. The crystal field analysis was performed to demonstrate the anisotropic magnetic behavior of $Ce@C_{82}$, relative to the crystal field in the cage.

2. Experimental Section

Details of the preparation of the endohedral metallofullerenes—$Ce@C_{82}$,[18,19] $La@C_{82}$,[20−22] and $Gd@C_{82}$[9,13]—were reported elsewhere.[1,17,23] Carbon soot that contained various metallofullerenes was produced by the dc arc-discharge method. Graphite/M composite rods (where M = Ce, La, Gd; Toyo Tanso Co., Ltd.) were used for the positive electrode. $Ce@C_{82}$, $La@C_{82}$, and $Gd@C_{82}$ were extracted from the respective resultant soot. Pure samples of these metallofullerenes were obtained by the so-called multistage HPLC method,[1,24,25] using

* Authors to whom correspondence should be addressed. E-mail: minakuma@chem.titech.ac.jp, tenoki@chem.titech.ac.jp.
† Tokyo Institute of Technology.
‡ Nagoya University.

10.1021/jp0275600 CCC: $25.00
Published on Web 06/28/2003

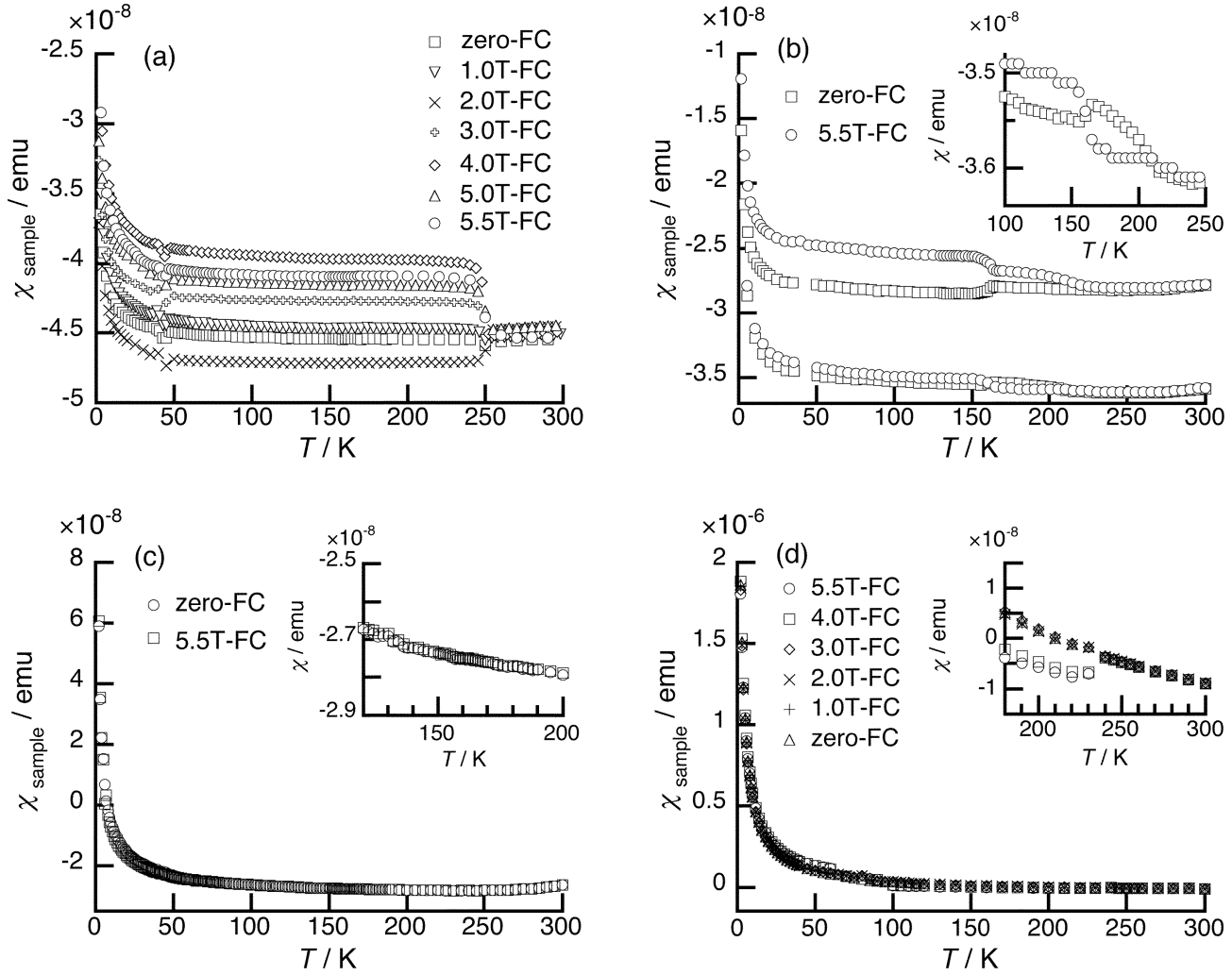

Figure 1. Magnetic susceptibility of the metallofullerenes in several solvents in the heating runs after field cooling and zero-field cooling processes. Panel a shows data for Ce@C_{82} in *o*-xylene solution (4.0×10^{-8} mol/0.07 mL); the freezing point of *o*-xylene is 248 K. Panel b shows data for Ce@C_{82} in CS_2 solutions (upper, 3.9×10^{-8} mol/0.04 mL; lower, 5.1×10^{-8} mol/0.05 mL); the inset is the enlarged illustration of the lower portion in the temperature range of 100−250 K, and the freezing point of CS_2 is 162 K. Panel c shows the Ce@C_{82} precipitates in diethyl ether (2.9×10^{-7} mol/0.05 mL); the inset is a magnified view in the temperature range of 120−200 K, and the freezing point of diethyl ether is 157 K. Panel d shows data for Gd@C_{82} in *o*-xylene solution (8.9×10^{-7} mol/0.06 mL); the inset is an enlarged illustration around the freezing point of *o*-xylene.

the recycling separations with several types of columns. The purity was confirmed using a laser desoprtion−time-of-flight (LD−TOF) mass spectrometer.

For solid film measurements, Ce@C_{82} or La@C_{82} film was prepared by the deposition of its solution saturated in carbon disulfide (CS_2) into a quartz cell. Each solid film in the quartz cell was sealed after heat treatment in a vacuum at 573 K for 24 h to remove the solvent in the film. The masses of Ce@C_{82} and La@C_{82} in the film were 1.0 ± 0.2 and 0.6 ± 0.2 mg, respectively. It should be noted that large errors were unavoidable in the weight measurement, because of the smallness of the sample amounts available in the measurements and the ambiguity introduced in the film sample formation. For solution measurements, the metallofullerenes in the solvents were also sealed in quartz cells in a vacuum after degassing dissolved oxygen gas in the solutions with the freeze−pump−thaw technique. The quantities of the metallofullerenes and the volumes of the solutions were as follows: Ce@C_{82}/*o*-xylene, 4.0×10^{-8} mol/0.07 mL; Ce@C_{82}/CS_2, 3.9×10^{-8} mol/0.04 mL, 5.1×10^{-8} mol/0.05 mL; Ce@C_{82}/diethyl ether, 2.9×10^{-7} mol/0.05 mL; Gd@C_{82}/*o*-xylene, 4.4×10^{-8} mol/0.05 mL, 8.9×10^{-7} mol/0.06 mL. All samples have traces of precipitates in their solutions (the amount of which is dependent on the solution), except the diethyl ether solution, for which a large fraction of sample is precipitated, even at room temperature. The concentrations of metallofullerenes in the solutions were also estimated from the magnetic moments ($J = {}^5/_2$ for Ce@C_{82}, $S = {}^7/_2$ for Gd@C_{82}) that were detected by the magnetic susceptibility measurement and the literature values of the diamagnetic susceptibilities of the solvents, because it was difficult to estimate them, because of the limited amounts of samples and the uncertainty of the region in the solution that was detectable in the magnetic measurements. The temperature dependence of the magnetic susceptibility was measured using SQUID equipment (Quantum Design, model MPMS-5) at 1.0 T over the temperature range of 2−300 K. The magnetization of the samples was measured in the magnetic field from −5.5 to 5.5 T at temperatures of 2, 60, and 200 K. The susceptibility data of the samples were obtained by subtracting the contribution of the quartz cell background from that of the samples via the SQUID response curve fitting.[26]

3. Results

The obtained susceptibilities of the *o*-xylene solutions of Ce@C_{82} over a temperature range of 2−300 K are shown in Figure 1a, where the data were taken in the heating run after

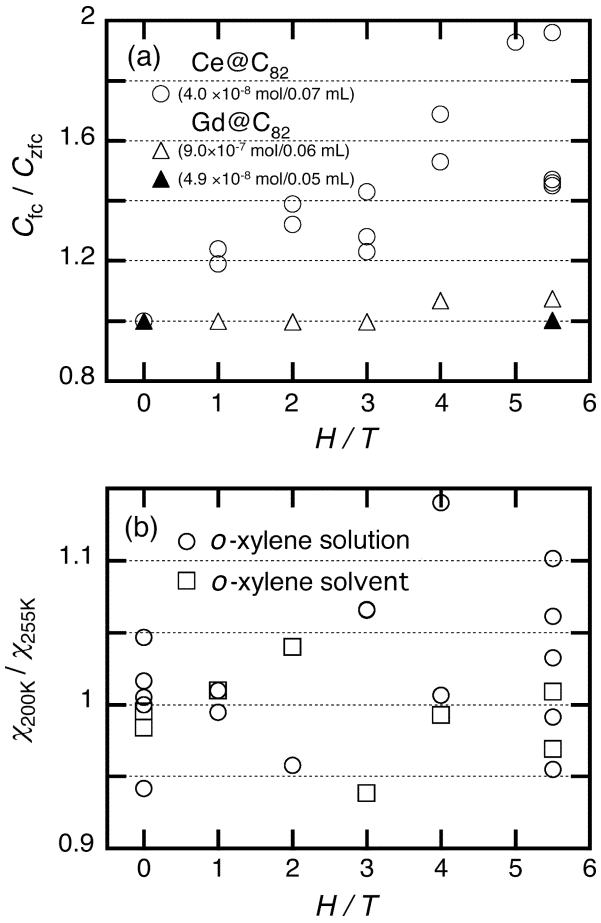

Figure 2. (a) Curie constant C_{fc} (open circles) versus applied field for Ce@C_{82} in the *o*-xylene solution in the field cooling experiments, where the Curie constant is estimated in the temperature range of 2−200 K. The Curie constant is normalized with respect to that in the zero-field cooling experiment (C_{zfc}). For comparison, the Curie constant data (triangles) of the solutions of Gd@C_{82} with isotropic magnetic properties are also shown. (b) Susceptibilities of the frozen state at 200 K (χ_{200K}) in the field cooling experiments for the *o*-xylene solution of Ce@C_{82} and the *o*-xylene solvent; the susceptibility is normalized with respect to that of the liquid state at 255 K (χ_{255K}).

the cooling processes in the absence or the presence of a magnetic field. Around the freezing temperature of *o*-xylene at 248 K, the susceptibility value showed a vertical shift discontinuously in the thawing processes, irrespective of cooling conditions between the field cooling and zero-field cooling measurements. The variation of the value was independent of the applied field magnitude. The susceptibilities of the CS_2 solutions of Ce@C_{82} are shown in Figure 1b. An abrupt increase in the susceptibility appeared at ∼165 K, which corresponded to the freezing point (162 K) of the CS_2 solvent when the sample was cooled under a magnetic field. In addition, another anomaly was sometimes observed at ∼220 K in the field cooling and zero-field cooling measurements. In contrast, the frozen diethyl ether solvent with the precipitates of Ce@C_{82} (note that Ce@C_{82} is actually insoluble in diethyl ether) had less variation in the susceptibility around the freezing point (157 K) of diethyl ether (Figure 1c). The susceptibility of Gd@C_{82} in *o*-xylene solutions also exhibited a discontinuous change at ∼240 K (Figure 1d). The order of this variation was not so different from that of Ce@C_{82} in *o*-xylene solution.

For all the Ce@C_{82} samples in three solvents, the Curie contribution in the susceptibility, which became divergent upon the decrease in the temperature, was found to be dependent on the field magnitude, when they were frozen in the applied field.

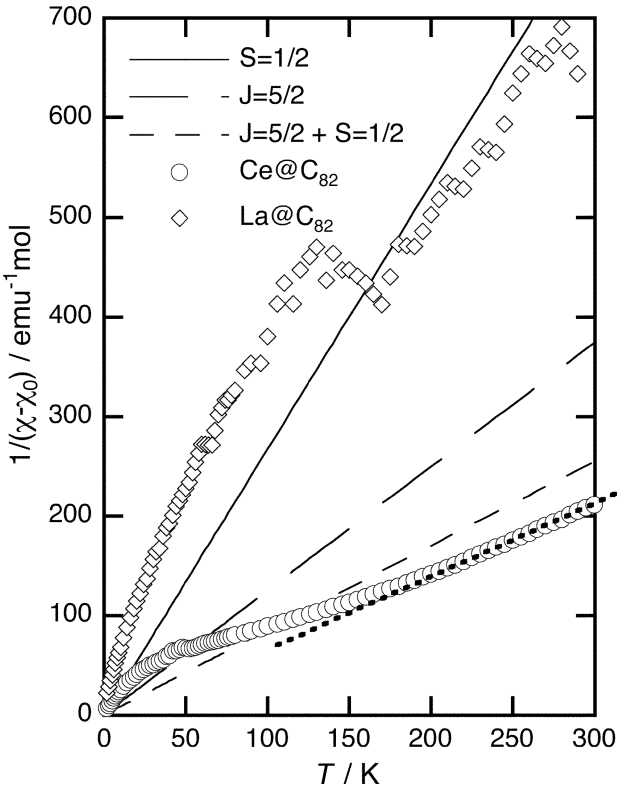

Figure 3. Reciprocal magnetic susceptibility of (○) Ce@C_{82} and (◇) La@C_{82} in solid film form. The solid line, the long dashed line, and the short dashed line show the susceptibilities for the free π-electron spin ($S = {}^1/_2$, $g_e = 2.0023$), the free Ce^{3+} ion ($J = {}^5/_2$, $g_J = 6/7$), and the sum of the free Ce^{3+} ion and the free π-electron spin, respectively. The dotted line represents the Curie−Weiss fitting of Ce@C_{82}, with $\Theta = -1$ K at temperatures above 180 K.

To investigate the magnetic behavior of Ce@C_{82} and Gd@C_{82} below the freezing point in the field cooling experiments, we apply the Curie−Weiss law (eq 1) to the temperature-dependent susceptibility in those solutions:

$$\chi - \chi_0 = \frac{C}{T - \Theta} \tag{1}$$

where χ_0 is the temperature independent term, C the Curie constant, and Θ the Weiss temperature. Figure 2a shows plots of the Curie constant versus the applied field for the *o*-xylene solutions of Ce@C_{82} and Gd@C_{82} in the field cooling experiments, where the Curie constant (C_{fc}) is normalized with respect to that in the zero-field cooling experiment (C_{zfc}). In the case of Ce@C_{82}/*o*-xylene, the normalized Curie constant C_{fc}/C_{zfc} increased upon elevation of the applied magnetic field and approached a value of ∼1.5−2 at a magnetic field strength of 5.5 T. The increase in the normalized Curie constant in the *o*-xylene solution was enhanced in subsequent measurements that were conducted several days after the first measurement. For Ce@C_{82}/CS_2 and Ce@C_{82}/(diethyl ether) solutions, the similar increase in the normalized Curie constant was found, where the value of C_{fc}/C_{zfc} was estimated as 1.2−1.3 and 1.1, respectively, at a magnetic field strength of 5.5 T. In contrast to the case of Ce@C_{82} solutions, no appreciable increase in the Curie constant was observed in the *o*-xylene solution of Gd@C_{82}, even if we increased the concentration of the solution by a factor of 15, as shown in Figure 2a.

The reciprocal magnetic susceptibilities of Ce@C_{82} and La@C_{82} in the solid film are shown as a function of temperature in Figure 3. The form of the sample was conserved throughout

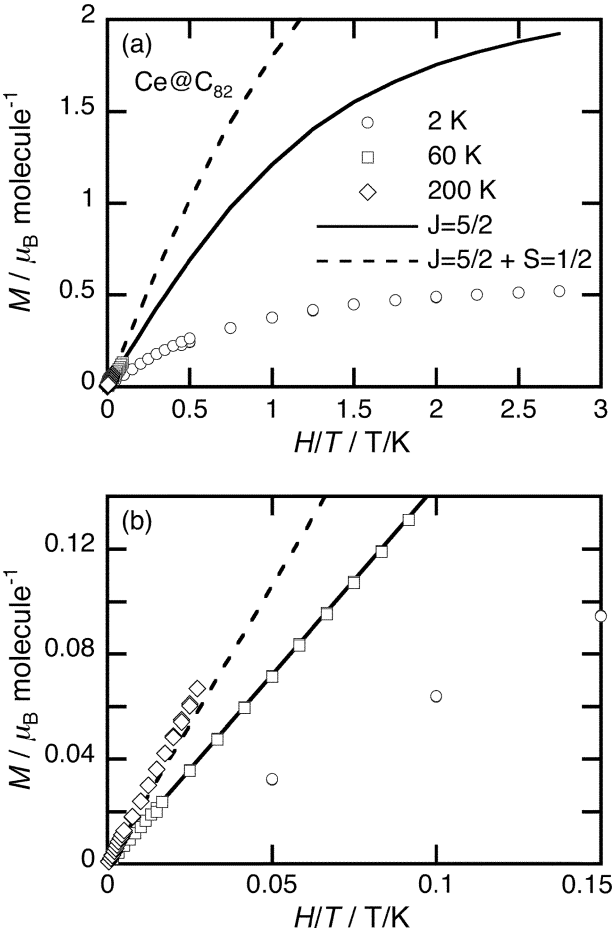

Figure 4. (a) Isothermal magnetization as a function of H/T at 2, 60, and 200 K in a solid film of Ce@C_{82} ((—) Brillouin curve with $J = {}^5/_2$ ($g_J = {}^6/_7$) and (- - -) sum of the Brillouin curves with $J = {}^5/_2$ ($g_J = {}^6/_7$) and with $S = {}^1/_2$ ($g_e = 2.0023$)). (b) Enlarged illustration of panel a in the low-field range.

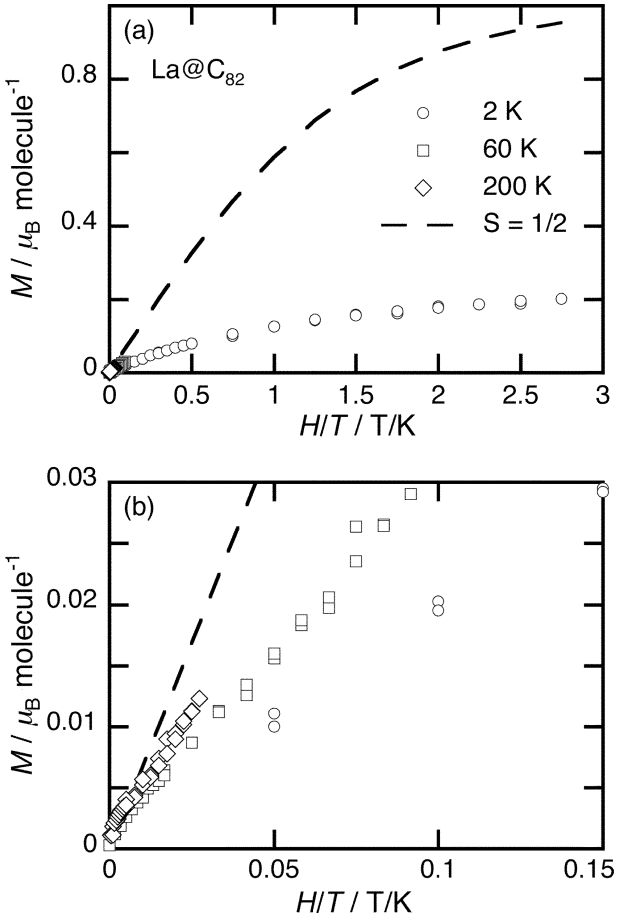

Figure 5. (a) Isothermal magnetization as a function of H/T at 2, 60, and 200 K in a solid film of La@C_{82}; the dashed line denotes the Brillouin curve with $S = {}^1/_2$ ($g_e = 2.0023$). (b) Enlarged illustration of panel a in the low-field range.

the experiment, so that the unexpected magnetization behavior by the crystal moving or rotating was negligible. The reciprocal susceptibility of Ce@C_{82} versus T plot did not fully obey the Curie−Weiss law over the entire temperature range investigated. It deviated from the Curie−Weiss behavior below ca. 180 K and exhibited a convex curvature below 50 K. The reciprocal susceptibility of La@C_{82} also exhibited a deviation from the Curie−Weiss law. It had a large anomaly at ∼150 K that was due to a crystal phase transition.[8,27] These deviations from the Curie−Weiss law and the presence of anomalies are similar to the behavior of the solvent-including crystal, Ce@$C_{82}(CS_2)_{1.5}$ and La@$C_{82}(CS_2)_{1.5}$, observed by Nuttall et al.[10] The Curie−Weiss fittings of the obtained susceptibilities gave small negative Weiss temperatures of $\Theta \approx -1$ and -10 K, respectively, in the higher-temperature region (>190 K for Ce@C_{82} and >170 K for La@C_{82}).

The magnetization curves of Ce@C_{82} and La@C_{82} at 2, 60, and 200 K in solid films are shown as a function of H/T in Figures 4 (Ce@C_{82}) and 5 (La@C_{82}). No hysteresis loop was observed at each temperature in the isothermal magnetization process. The magnetization curves as a function of H/T took different traces, depending on the temperature. The magnetization curve of Ce@C_{82} went over the magnetization curve of the free Ce^{3+} ion at 200 K. The curve tracked that of the free spin Ce^{3+} ion at 60 K, and then its value became ∼3 times less than that of a free Ce^{3+} ion ($J = {}^5/_2$, $g_J = {}^6/_7$) at $H/T = 3$ with 2.0 K. In contrast, the magnetization curve of La@C_{82} went below the magnetization curve of the free π-electron spin, even at 200 K. Its value was ∼5 times less than that of a free π electron ($S = {}^1/_2$, $g_e = 2.0023$) at $H/T = 3$ with 2.0 K.

4. Discussion

The first portion of the discussion is devoted to the magnetic behavior of the solution states. The discontinuous variations of the susceptibility value around the freezing temperature of the solutions shown in Figure 1 are considered to be caused mainly by the diamagnetic anisotropy of the solvent molecules. The ratio of the susceptibility change between liquid (255 K) and frozen (200 K) conditions, χ_{220K}/χ_{255K}, is shown as a function of the applied field in Figure 2b for the *o*-xylene solution of Ce@C_{82} and the pure *o*-xylene solvent. The similarity in the variation of the susceptibility between the solution and the pure solvent is held independent of the applied field magnitude. The amount (0.07 mL) of the *o*-xylene used in the Ce@C_{82} solution is expected to give a difference of up to 3.9×10^{-8} emu in the diamagnetic susceptibility between the field directions parallel and perpendicular to the molecular plane, taking into account the reported anisotropy (68.0×10^{-6} emu mol^{-1}).[28] The largest difference in the present study, 0.7×10^{-8} emu, is ∼19% of the expected anisotropy. Therefore, these variations are caused by a subtle difference in the distribution of the orientations of small crystallites of solvent molecules, which can be easily varied by the environment when *o*-xylene is frozen. This observation also well explains the result that the susceptibility variations of the Gd@C_{82} and Ce@C_{82} samples in *o*-xylene are not so different, despite the large difference in the magnetic

moments and the anisotropy of the interior metal ions. As we will see later with the calculation of magnetic susceptibility, the difference in the susceptibility of $Ce@C_{82}$ between the easy-axis and the hard-axis directions at 250 K ($\Delta\chi = 8.8 \times 10^{-10}$ emu) is much less than that of *o*-xylene ($\Delta\chi = 3.9 \times 10^{-8}$ emu) at the same temperature, so that the contribution of $Ce@C_{82}$ to the magnetic anisotropy is not detectable in the discontinuous changes around the freezing point. Discontinuous changes of the solvent origin shown in Figure 1b are also observed at the freezing point for the CS_2 samples (165 K), despite the smaller diamagnetic anisotropy of CS_2 (14.0×10^{-6} emu mol^{-1})[28] than that of *o*-xylene. In addition, another anomaly is observed at ~220 K in the CS_2 solution of $Ce@C_{82}$, which is absent in pure CS_2 solvent. The origin is still an open question in regard to the anomaly at ~220 K. It is, however, considered that the magnetic anomaly can be related to the formation of the clusterlike structure between $Ce@C_{82}$ and CS_2 solvent molecules in the solution, as seen in CS_2 solution of C_{60}.[29] Further considering that the viscosity of the solution increases around the freezing point, short-range order develops with the formation of clusters in the critical region. It is, therefore, suggested that the magnetism of the $Ce@C_{82}-CS_2$ composite in the solution causes the anomaly at ~220 K. For the diethyl ether sample, diethyl ether has a negligible anisotropy in the susceptibility. In addition, $Ce@C_{82}$ crystals precipitated well above the melting point of the solvent (157 K) and hardly rotate in diethyl ether before freezing. Therefore, no field-induced variation of the susceptibility is expected, as observed in the experiment. (See Figure 1c.)

Here, we discuss the anisotropic magnetic feature in relation to the molecular and crystal structures of the metallofullerenes. The interior metal ion is located off-center of the spherical cage of the metallofullerene. Considering that the orbital angular momentum with the low-symmetry crystal field produces anisotropy in magnetism, $Ce@C_{82}$, where the Ce^{3+} ion has the orbital angular momentum $L = 3$ ($J = {}^5/_2$), is magnetically anisotropic, in contrast to isotropic $Gd@C_{82}$ with the Gd^{3+} ion, which has no orbital angular momentum ($S = {}^7/_2$). Therefore, the difference in the field dependence of the Curie constant can be explained on the basis of the preferred orientation of $Ce@C_{82}$ molecules that is induced by the applied field. However, as will be described later, the calculated magnetic energy difference at $T = 250$ K, $H = 1$ T between the spin easy axis and the spin hard axis of a $Ce@C_{82}$ molecule ($\Delta E_{250\ K} = {}^1/_2\Delta\chi H^2 = 5.2 \times 10^{-4}$ K, where $\Delta\chi = \chi_{||C_2} - \chi_{\perp C_2}$) is considerably small, compared to the thermal energy, where the spin easy axis of the f electron in $Ce@C_{82}$ is aligned parallel to the C_2-axis, according to the calculation. Assuming that the spin easy axes of $Ce@C_{82}$ are oriented in the same direction for all the molecules associated in the cluster, clustering can make the rotational motion easily take place, because of the large reduction in the rotational energy. For example, the rotational energy of a cubic-shaped cluster, including eight $Ce@C_{82}$ molecules (radius of 5.5 Å, weight of 1124 amu), is estimated at 3×10^{-4} K, which is comparable to the magnetic anisotropy energy. Actually, it is reported that mono metallofullerenes align with their C_2-axes of the cages oriented to the same direction in the crystal, even at room temperature, because of their large electric dipole moments.[5−8] The dipole−dipole interaction between the metallofullerenes is responsible for the uniaxial orientation of the metallofullerenes. In the vicinity of the freezing point ($T \geq T_f$), clusters of $Ce@C_{82}$ molecules develop in concert with the aid of the dipole−dipole interaction. Therefore, the increase in the Curie constant upon the increase in the magnetic field in the field cooling process can be explained in terms of the rotation of the spin easy axis coupled to the cluster rotation. In the liquid state at high temperatures, clusters can rotate freely, where the direction of the magnetic moment can also be changed frequently by the thermal agitation. In the vicinity of the freezing temperature, the applied magnetic field works to make the spin easy axis oriented to the field direction against thermal agitation, resulting in the preferred cluster orientations. This effect becomes more effective as we move more toward the freezing point, because the cluster motion becomes extremely decelerated. Furthermore, this effect is enhanced when the cluster size is large at high fullerene concentrations, because the long-range dipole−dipole interaction works to make molecular orientation cooperatively. The time-dependent increase in the Curie constant of the *o*-xylene solution of $Ce@C_{82}$, which we mentioned in the last section, is considered to be due to the growth of the $Ce@C_{82}$ cluster in the solution as time passes. No appreciable increase in the Curie constant of the $Gd@C_{82}$ solution is observed, even in the high concentration, which highlights the importance of the magnetic anisotropy of the metallofullerene. Below the freezing point, the cluster orientations achieved at the freezing point are quenched, resulting in the preferred orientation of the spin easy axes. This is the reason why the Curie constant increases more for the sample that was field-cooled at a higher applied field.

Next, we discuss the magnetism of the samples in the solid state. In the higher-temperature region, the Curie−Weiss behavior with a small Weiss temperature is observed, as shown in Figure 3. Therefore, the magnetic structure of the metallofullerenes can be described by a simple summation of the free spin of the interior metal ion and that of the π electron on the cage, which are independent from each other, even in the solid state. Actually, the obtained Curie constants—1.42 and 0.42 emu mol^{-1} K for $Ce@C_{82}$ and $La@C_{82}$, respectively—correspond to those expected for the sum of a single 4f electron of the Ce^{3+} ion and a single π electron on the C_{82} cage ($0.803 + 0.385 = 1.19$ emu mol^{-1} K) and to a single π electron on the C_{82} cage (0.385 emu mol^{-1} K). (The differences of the Curie constants between the experiment and the calculation are considered to be due to experimental errors in limited amounts of the samples in the measurements.) The Curie constants in the present study are approximately the same as those of the solvent-including crystal reported by Nuttall et al.[10] (1.33 emu mol^{-1} K for $Ce@C_{82}(CS_2)_{1.5}$, 0.46 emu mol^{-1} K for $La@C_{82}(CS_2)_{1.5}$). The difference between the present result and the previous one[10] is observed in the Weiss temperature at >200 K. The solvent-including crystal has a large negative Weiss temperature[10] ($\Theta \approx -110$ K for $Ce@C_{82}(CS_2)_{1.5}$, $\Theta \approx -130$ K for $La@C_{82}(CS_2)_{1.5}$), in contrast to the small negative temperatures for the solvent-free crystal in the present study. This difference of the Weiss temperatures comes from the point that the solvent molecules enhance the dimerization and the $\pi-\pi$ antiferromagnetic interaction between the metallofullerenes.

It should be discussed that the susceptibility deviates from the Curie−Weiss behavior at ~180 K for $Ce@C_{82}$ and ~170 K for $La@C_{82}$. The deviation is considered to be due to a transition that is related to the quenching of molecular rotation. Indeed, the solvent-free crystals, $Ce@C_{82}$[11] and $La@C_{82}$,[8] have phase transitions of molecular-rotation origin at ~150 K. The large deviation of the susceptibility of $La@C_{82}$ shown in Figure 3 suggests that the quenching molecular rotation enhances the antiferromagnetic exchange interaction between the π-electron spins on the neighboring cages. In contrast, only a small deviation in $Ce@C_{82}$ appears below ~180 K, although the

change of the intermolecular $\pi-\pi$ interaction of Ce@C_{82} is considered to occur at the transition similar to La@C_{82}. The different behavior of Ce@C_{82} from that of La@C_{82} is considered to be due to the existence of the spin of the interior metal ion. In the free-spin model, the contribution of the magnetic moment of Ce ion, $\mu_{\text{eff}}[Ce^{3+}]$, is ~68% to the susceptibility of Ce@C_{82}. Therefore, a large contribution of the magnetic moment of the Ce ion makes the change in the susceptibility of the π-electron spin less observable. This contribution of the magnetic moment of the interior ion to the susceptibility can explain the previous results of the heavy rare-earth metallofullerenes (Gd, Tb, Dy, Ho, Er),[14,15] where the deviation from the Curie−Weiss law and the presence of the phase-transition-induced discontinuities have not been observed at >50 K. The contribution of the magnetic moment of those heavy rare-earth ions is >95%, which makes the magnetic variation of the π-electron spins negligible. Further reduction of the temperature pronounces the deviation of the susceptibility of Ce@C_{82} from the Curie−Weiss behavior, as can be seen in Figure 3. Taking into account that no phase transition takes place at <130 K,[11] the convex curvature in the $1/\chi$ vs T curve below ca. 50 K is considered to be caused by the crystal field effects, which induces the magnetic anisotropy of Ce@C_{82}.

The magnetization, M, does not fully obey the Brillouin function of the free spins, as shown in Figures 4 and 5, for Ce@C_{82} and La@C_{82}, respectively. The obtained magnetic moment at 2 K (0.2 μ_B), is less than the first reported value for La@C_{82} by Funasaka et al.[9] (0.38 μ_B), even taking the error in the weight measurement of the sample into account (Figure 5). They estimated the magnetic moment from the Curie constant, which was obtained by the temperature dependence of the reciprocal susceptibility at 5 T, from 5 K to 40 K. In the large field and the short temperature region at the low temperatures, it is difficult to apply the molecular field approximation to estimating the magnetic moment. On the other hand, we obtained the magnetic moment, 0.2 μ_B, from the magnetization curve at 2 K. The difference of the present magnetic moment from Funasaka's value is considered to originate from the estimating procedure for the magnetic moment. The magnetization curves of La@C_{82} are below the magnetization curve of the free electron spin ($S = {}^1/_2$), and the value at 2 K and 5.5 T is ~5 times less than that of a free π electron. This observation suggests an important role of the antiferromagnetic interaction between the π-electron spins on the adjacent cages, which is also evidenced by the reduction of the susceptibility that appears below the transition temperature (at ~170 K). In contrast, the magnetization curve of Ce@C_{82} at 200 K is in good agreement with that expected with the summation of the magnetizations of the free spin of the Ce^{3+} ion and the π-electron spin, suggesting the minor contribution of the $\pi-$f and $\pi-\pi$ interactions at high temperatures, consistent with the small Weiss temperature. The magnetization curve ($M-(H/T)$ plot) of Ce@C_{82} becomes less steep as the temperature decreases, which indicates the increasing contribution of the $\pi-$f antiferromagnetic interaction, in addition to the $\pi-\pi$ interaction, as suggested in La@C_{82}. According to the recent W-band EPR study for Gd@C_{82},[30] it has been reported that the f spin of the interior Gd^{3+} ion of the Gd@C_{82} monomer is weakly antiferromagnetically coupled with the π spin on the cage ($E_{ex} \approx -8$ K). It has been also reported that the π spin on the cage of Gd@C_{82} has an antiferromagnetic interaction with that of the neighboring molecule in the solid state and in the dimer state, so that the spin state of Gd@C_{82} is approximately described as $S = {}^7/_2$ (Gd^{3+}); the π spins are quenched because of the formation of an antiparallel arrangement at low temperatures. It is natural that Ce@C_{82} is considered to have the $\pi-$f and $\pi-\pi$ interactions in the range that is similar to those in Gd@C_{82}. Eventually, the magnetization of Ce@C_{82} at 2 K, where the magnetization is ~3 times less than that of a free Ce^{3+} ion, can be explained by the $\pi-$f and $\pi-\pi$ interactions, which become less important in the intermediate temperature range well above 10 K. In other words, the crystal field effect has an important role in the magnetic behavior in the intermediate temperature range.

Considering the crystal field effect, the knowledge of the environment surrounding the electrons in the interior metal ion is important. For La@C_{82}, the interior metal La^{3+} ion moves hemispherically, with a large amplitude of 2−2.5 Å from the equilibrium position inside the C_{82} cage at room temperature; that is, the La^{3+} ion is distributed similar to a bowl along the interior wall of the cage.[7] This means that the potential energy barrier for the La ion is quite shallow in the cage. The calculated free energy barrier at room temperature is reported[31] to be ~10 kcal mol^{-1}. The Ce ion in Ce@C_{82} can be also considered to move hemispherically, as well as the La ion in La@C_{82}, because of the similar electronic[17,32] and vibrational[33] state for each ion. For the large amplitude motion of the encapsulated metal ion, the crystal field of the cage to the interior metal ion becomes thermal averaged, resulting in a reduction of the crystal field effect. Therefore, the precise crystal field analysis can be applied to the obtained susceptibility only in the low-temperature region well below the crystal field splitting energy.

We analyze the susceptibility data on the basis of the crystal field theory[34−37] for Ce@C_{82}. The $^2F_{5/2}$ ground-state multiplet of a free Ce^{3+} ion splits into three Kramers doublets under the crystal field of a local symmetry that is lower than a cubic one. We make the following assumptions. First, Ce@C_{82} has the electronic structure with a $4f^1$ spin on the Ce^{3+} ion and a π-electron spin on the cage. Second, a Ce^{3+} ion in Ce@C_{82} is located at the off-center position along the C_2-axis of the C_{82} cage, as shown in Figure 6. Third, the $\pi-$f and $\pi-\pi$ exchange interactions are negligible at the temperatures concerned. Finally, the anisotropy observed in the measured susceptibilities is uniaxial and, hence, we assume the crystal field of the interior cage to have tetragonal symmetry, neglecting an anisotropy in the vertical plane of the C_2-axis. The crystal field Hamiltonian $\hat{H}_{CF}$,[35,37] in this case, is written as

$$\hat{H}_{CF} = B_2^0 O_2^0 + B_4^0 O_4^0 + B_4^4 O_4^4 \tag{2}$$

where O_m^n are the Stevens operators and B_m^n are the crystal field parameters to be empirically evaluated. We consider the C_2-axis of the C_{82} cage to be the z-axis, and, hence, the total angular momentum operators are expressed as $J_{\parallel C_2} = J_z$ and $J_{\perp C_2} = J_x$. The eigenfunctions of the three Kramers doublets are expressed as

$$|1\pm\rangle = \cos\theta|\pm 5/2\rangle + \sin\theta|\mp 3/2\rangle \tag{3}$$

$$|2\pm\rangle = \sin\theta|\pm 5/2\rangle - \cos\theta|\mp 3/2\rangle \tag{4}$$

$$|3\pm\rangle = |\pm 1/2\rangle \tag{5}$$

where θ takes values in the region $0 \le \theta \le \pi/2$, which is calculated from B_m^n, so as to diagonalize the Hamiltonian (eq 2). The energy eigenvalues of each state are expressed as

$$E_1 = \langle 1\pm|\hat{H}_{CF}|1\pm\rangle \tag{6}$$

$$E_2 = \langle 2\pm|\hat{H}_{CF}|2\pm\rangle \tag{7}$$

$$E_3 = \langle 3\pm|\hat{H}_{CF}|3\pm\rangle \tag{8}$$

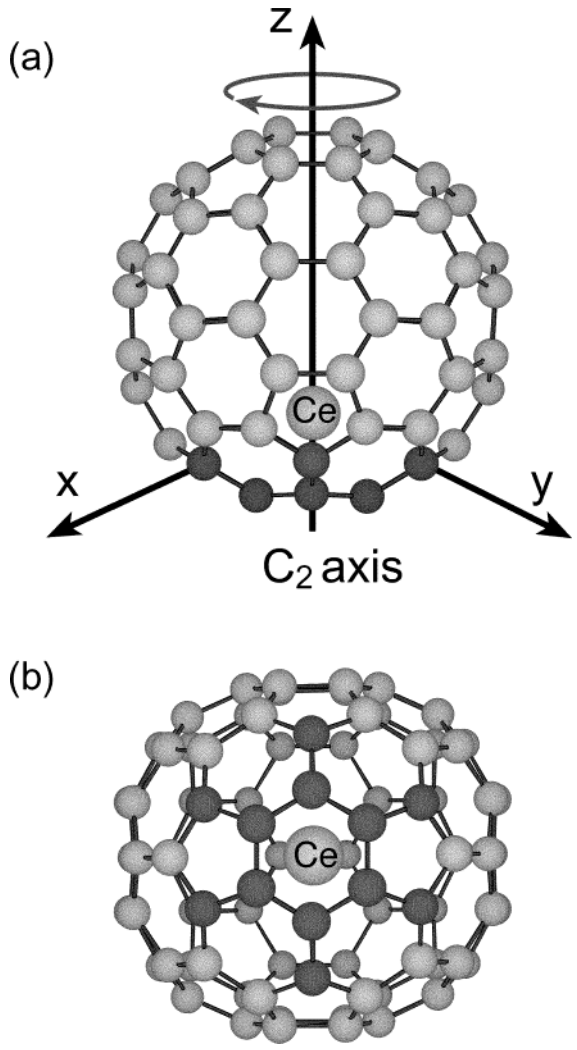

Figure 6. Molecular structure of Ce@C_{82} with a C_{2v} symmetry cage. Panel a shows a side view, where the large sphere and small spheres are Ce and C atoms, respectively; panel b shows the bottom view. The metal ion is displaced from the center of the cage and is located adjacent to the center of a six-membered ring of the cage. The first- and second-nearest-neighbor C atoms from the Ce atom have a hexagonal symmetry.

The susceptibility χ_α can be calculated from the following formula:

$$\chi_\alpha = \frac{N_A g_J^2 \mu_B^2}{k_B Z_0}\left(\sum_{i,k}^{E_i=E_k}\left|\langle k|J_\alpha|i\rangle\right|^2\left[\frac{\exp(-E_k/T)}{T}\right] + \sum_{i,k}^{E_i\neq E_k}\left|\langle k|J_\alpha|i\rangle\right|^2\left[\frac{\exp(-E_k/T)-\exp(-E_i/T)}{E_i-E_k}\right]\right) \quad (9)$$

where Z_0, the partition function, is

$$Z_0 = \sum_i \exp\left(\frac{-E_i}{T}\right) \quad (10)$$

and $\alpha = \|C_2$ or $\perp C_2$ for the susceptibility parallel or perpendicular to the C_2 axis of Ce@C_{82}, respectively. N_A is the Avogadro's number, g_J the Landé factor (which is $^6/_7$ for the $^2F_{5/2}$ multiplet), and E_i the energy of the crystal field eigenfunction $|i\rangle$ ($i = 1\pm, 2\pm, 3\pm$). Note that $E_{1+} = E_{1-}$, $E_{2+} = E_{2-}$, and $E_{3+} = E_{3-}$.

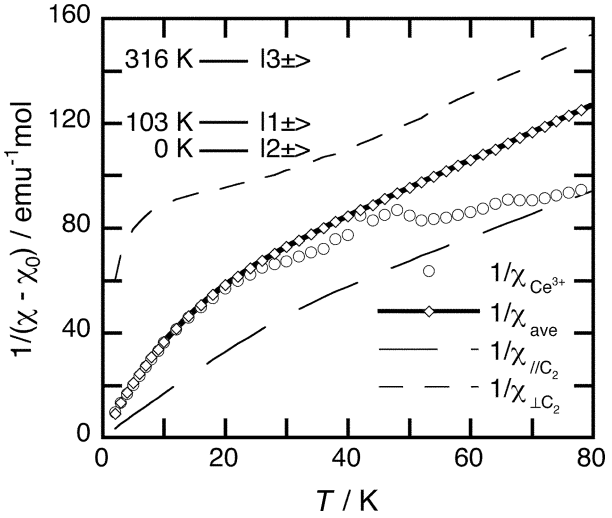

Figure 7. Reciprocal magnetic susceptibility of the contribution of the Ce^{3+} f electron experimentally obtained from $\chi_{Ce@C_{82}} - \chi_{La@C_{82}}$ (open circles) and the crystal field analyses. The solid line with diamonds is the average of the calculated susceptibility for the Ce^{3+} f electron using the crystal field parameters (see text). The crystal-field level scheme is also shown.

The averaged crystal-field dependent susceptibility for the nonoriented film form sample, where small crystallites are randomly oriented, is given as

$$\chi_{ave} = \frac{1}{3}\chi_{\|C_2} + \frac{2}{3}\chi_{\perp C_2} \quad (11)$$

Using the crystal field parameters as adjustable parameters, the experimental data are fitted with eq 11. It is reasonably assumed that the π electron on the Ce@C_{82} cage has the same magnetic behavior as that of La@C_{82}, where the susceptibility contribution of the π electron can be represented by the susceptibility of La@C_{82} ($\chi_{La@C_{82}}$). Therefore, the susceptibility contribution of the f-electron spin of the Ce^{3+} ion, $\chi_{Ce^{3+}}$, is obtained by $\chi_{Ce@C_{82}} - \chi_{La@C_{82}}$.

The calculated crystal field parameters are obtained by fitting with the experimental results below 40 K ($B_2^0 = -9.0$ K, $B_4^0 = 0.87$ K, $B_4^4 = 0.38$ K, $\cos\theta = 0.99$, $\sin\theta = 0.10$). The energy differences are given as 103 and 316 K for $|1\pm\rangle$ and $|3\pm\rangle$, respectively, from the ground state $|2\pm\rangle$. The calculated susceptibility, χ_{ave}, reproduces the observed convex curvature below 50 K well, as shown with the experimental data in Figure 7. The spin easy axis of the f electron is aligned parallel to the C_2-axis according to the calculation. The difference of the susceptibility between the spin easy axis and the spin hard axis, $\Delta\chi = \chi_{Ce@C_{82}} - \chi_{La@C_{82}}$, increases as the temperature decreases. The obtained parameters $\cos\theta$ and $\sin\theta$ are almost 1 and 0, respectively. Consequently, the eigenfunctions of the three Kramers doublets are expressed as $|\pm^5/_2\rangle$, $|\pm^3/_2\rangle$ and $|\pm^1/_2\rangle$, suggesting a hexagonal feature in the crystal field of the cage at low temperatures. The hexagonal crystal field analysis in the present study gives the result that the ground state of the f-electron spin of the Ce^{3+} ion is $|\pm^3/_2\rangle$. It is reasonable that the hexagonal crystal field at low temperatures can affect the Ce^{3+} ion, because the metal ion locates adjacent to the center of a six-membered ring of the cage at low temperature, as shown in Figure 6b. The growing deviation of the theoretical curve from the experimental data above ca. 50 K indicates that the thermally excited motion of the metal ion becomes pronounced as the temperature is elevated. Therefore, the crystal field from the cage is successively modified at high temperatures.

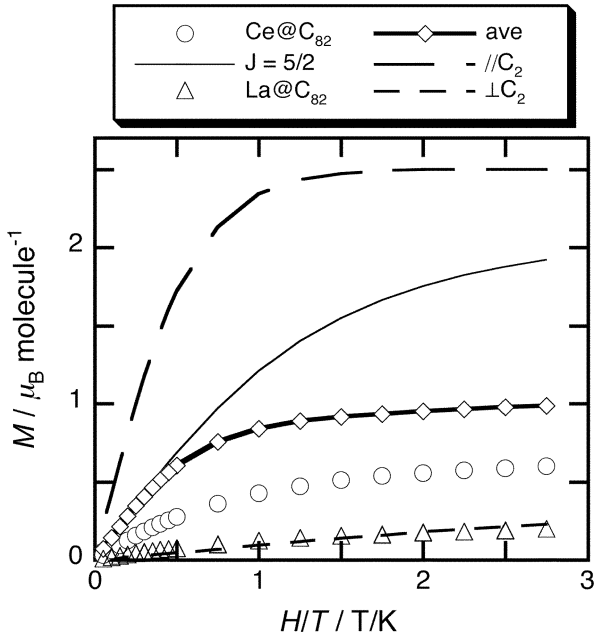

Figure 8. Observed magnetization of $Ce@C_{82}$ (open circles) and $La@C_{82}$. The plot calculated from the crystal field analyses, as a function of H/T at 2 K, is shown for $Ce@C_{82}$, where the long and short dashed lines represent the magnetization curves of spin easy axis ($\parallel C_2$) and hard axis ($\perp C_2$), respectively. The average magnetization (thick solid line with diamonds) is given by $M_{ave} = {}^1/_3(M_{\parallel} + 2M_{\perp})$. For comparison, the Brillouin curve of the free Ce^{3+} ion ($J = {}^5/_2$, $g_J = {}^6/_7$) is also shown.

The magnetization curve of $Ce@C_{82}$ at 2 K is shown with the curves calculated with the ground spin state of $Ce@C_{82}$ in Figure 8. From the calculated results, the first excited state $|1\pm\rangle$ is located 103 K above the ground-state doublet $|2\pm\rangle$. Therefore, only the ground state contributes to the magnetization at 2 K. The magnetization experimentally obtained is in approximate agreement with that calculated, although the former is still lower than the later. The $\pi-$f interaction is considered to contribute to the difference. In other words, the present result proves that the crystal field and the antiferromagnetic $\pi-$f exchange interaction between the cage and the metal are essential in the magnetic nature of the metallofullerenes at low temperatures.

Finally, it should be noted that the crystal field splittings (103 K, 306 K) are considerably reduced in comparison with those of ordinary cerium compounds. This suggests that the Ce atom is weakly bound to the C_{82} cage, which is consistent with the small hyperfine field observed in $La@C_{82}$.[20−22]

5. Conclusions

Cerium endohedral metallofullerene ($Ce@C_{82}$) is an unconventional $\pi-$f composite nanomagnet, where the anisotropic f-electron spin is expected to be coupled with the rotational motion of the fullerene cage that has π-electron spin. We have investigated the magnetic properties of $Ce@C_{82}$ by examining the field-induced change in the magnetic susceptibility of organic solutions of $Ce@C_{82}$ and the temperature dependence of the magnetic susceptibility and magnetization of $Ce@C_{82}$ solid films. The field cooling effect on the susceptibility of $Ce@C_{82}$ in organic solutions suggests that the application of magnetic field makes the molecular orientations become aligned, in cooperation with the magnetic anisotropy of the f-electron spin coupled with the molecular orientation, resulting in the preferred orientations of fullerene molecules in the frozen solution under the magnetic field. The role of crystal field to the magnetic anisotropy, which is associated with the off-centered geometry of the Ce ion in the cage, is clarified by the crystal field analysis of the temperature dependence of the susceptibility. The crystal field effect is considerably reduced to the range of 100−300 K, in contrast to that of ordinary rare-earth compounds, which is consistent with the findings of a small electronic coupling between the f and π electrons and the shallow potential of the surrounding cage to the Ce ion. As a consequence, the crystal field effect is emphasized in the intermediate temperature range below ~100 K. At low temperatures, the magnetism is subjected to the cooperation of an intramolecular $\pi-$f interaction and an intermolecular $\pi-\pi$ interaction, in addition to the crystal field effect.

Acknowledgment. The authors would like to thank Prof. K. Suzuki (Yokohama National University) and Prof. N. Kojima (University of Tokyo) for valuable discussions. The authors also express their cordial gratitude to Dr. N. Ishikawa (Tokyo Institute of Technology) for helpful suggestions for the crystal field analysis. The authors also appreciate valuable discussions with Prof. T. Kato and Dr. K. Kobayashi (IMS). H.S. thanks the JSPS Future Program on New Carbon Nano-Materials. T.E. thanks the JSPS Future Program on Basic Science and Applications of Nanocarbons Developed for Advanced Energy Devices for the financial support of the present study.

References and Notes

(1) Shinohara, H. *Rep. Prog. Phys.* **2000**, *63*, 843.
(2) Laasonen, K.; Andreoni, W.; Parrinello, M. *Science* **1992**, *258*, 1916.
(3) Kobayashi, K.; Nagase, S. *Chem. Phys. Lett.* **1998**, *282*, 325.
(4) Nagase, S.; Kobayashi, K. *Chem. Phys. Lett.* **1993**, *214*, 57.
(5) Nishibori, E.; Takata, M.; Sakata, M.; Inakuma, M.; Shinohara, H. *Chem. Phys. Lett.* **1998**, *298*, 79.
(6) Takata, M.; Umeda, B.; Nishibori, E.; Sakata, M.; Saito, Y.; Ohno, M.; Shinohara, H. *Nature* **1995**, *377*, 46.
(7) Nishibori, E.; Tanaka, M.; Sakata, M.; Tanaka, H.; Hasegawa, M.; Shinohara, H. *Chem. Phys. Lett.* **2000**, *330*, 497.
(8) Watanuki, T.; Fujiwara, A.; Ishii, K.; Matsuoka, Y.; Suematsu, H.; Ohwada, K.; Nakao, H.; Fujii, Y.; Kodama, K.; Kikuchi, K.; Achiba, Y. *Mol. Cryst. Liq. Cryst. Sci. Technol. A* **2000**, *340*, 639.
(9) Funasaka, H.; Metals, K. S.; Yamamoto, K.; Takahashi, T. *J. Phys. Chem.* **1995**, *99*, 1826.
(10) Nuttall, C. J.; Inada, Y.; Nagai, K.; Iwasa, Y. *Phys. Rev. B* **2000**, *62*, 8592.
(11) Nuttall, C. J.; Watanabe, Y.; Inada, Y.; Nagai, K.; Muro, T.; Chi, D. H.; Takenobu, T.; Iwasa, Y.; Kikuchi, K. Structural and Magnetic Studies of the Endohedral Metallofullerene $Ce@C_{82}$. In *Electronic Properties of Novel Materials—Science and Technology of Molecular Nanostructures*; Kuzmany, H., Fink, J., Mehring, M., Roth, S., Eds.; American Institute of Physics: New York, 1999; Vol. 486, p 115.
(12) Nuttall, C. J.; Inada, Y.; Watanabe, Y.; Nagai, K.; Muro, T.; Chi, D. H.; Takenobu, T.; Iwasa, Y.; Kikuchi, K. *Mol. Cryst. Liq. Cryst. Sci. Technol. A* **2000**, *340*, 635.
(13) Funasaka, H.; Sakurai, K.; Oda, Y.; Yamamoto, K.; Takahashi, T. *Chem. Phys. Lett.* **1995**, *232*, 273.
(14) Huang, H. J.; Yang, S. H.; Zhang, X. X. *J. Phys. Chem. B* **1999**, *103*, 5928.
(15) Huang, H.; Yang, S.; Zhang, X. *J. Phys. Chem. B* **2000**, *104*, 1473.
(16) Wakahara, T.; Okubo, S.; Kondo, M.; Maeda, Y.; Akasaka, T.; Waelchli, M.; Kako, M.; Kobayashi, K.; Nagase, S.; Kato, T.; Yamamoto, K.; Gao, X.; Caemelbecke, E. V.; Kadish, K. M. *Chem. Phys. Lett.* **2002**, *360*, 235.
(17) Akiyama, K.; Sueki, K.; Kodama, T.; Kikuchi, K.; Ikemoto, I.; Katada, M.; Nakahara, H. *J. Phys. Chem. A* **2000**, *104*, 7224.
(18) Ding, J.; Yang, S. *Chem. Mater.* **1996**, *8*, 2824.
(19) Georgi, P.; Kuran, P.; Dunsch, L. Cerium Metallofullerenes. In *Electronic Properties of Novel Materials—Science and Technology of Molecular Nanostructures*; Kuzmany, H., Fink, J., Mehring, M., Roth, S., Eds.; American Institute of Physics: New York, 1999; Vol. 486, p 106.
(20) Johnson, R. D.; de Vries, M. S.; Salem, J.; Bethune, D. S. *Nature* **1992**, *355*, 239.
(21) Suzuki, S.; Kawata, S.; Shiromaru, H.; Yamaushi, K.; Kikushi, K.; Kato, T.; Achiba, Y. *J. Phys. Chem.* **1992**, *96*, 7159.

(22) Yamamoto, K.; Funasaka, H.; Takahashi, T.; Akasaka, T. *J. Phys. Chem.* **1994**, *98*, 2008.

(23) Fuchs, D.; Rietschel, H.; Michel, R. H.; Fischer, A.; Weis, P.; Kappes, M. M. *J. Phys. Chem.* **1996**, *100*, 725.

(24) Wang, C.-R.; Inakuma, M.; Shinohara, H. *Chem. Phys. Lett.* **1999**, *300*, 379.

(25) Inakuma, M.; Shinohara, H. *J. Phys. Chem. B* **2000**, *104*, 7595.

(26) Butzlaff, C. Subtracting the Sample Holder Background from Diluted Samples. In *Quantum States*; Quantum Design: San Diego, CA, 1994; p 1.

(27) Fujiwara, A.; Ishii, K.; Watanuki, T.; Suematsu, H.; Nakao, H.; Ohwada, K.; Fujii, Y.; Murakami, Y.; Mori, T.; Kawada, H.; Kikegawa, T.; Shimomura, O.; Matsubara, T.; Hanabusa, H.; Daicho, S.; Kitamura, S.; Katayama, C. *J. Appl. Crystallogr.* **2000**, *33*, 1241.

(28) *Diamagnetic Susceptibility*; Landolt−Börnstein Numerical Data and Functional Relationships in Science and Technology, New Series II/16; Springer: Berlin, 1986.

(29) Tomiyama, T.; Uchiyama, S.; Shinohara, H. *Chem. Phys. Lett.* **1997**, *264*, 143.

(30) Kato, T.; Furukawa, K.; Okubo, S.; Akasaka, T.; Kato, H.; Shinohara, H. ESR Study on Spin State of Gd@C_{82}. Presented at The 23rd Fullerene, Nanotubes General Symposium, July 17−19, 2002, Matsushima, Miyagi, Japan.

(31) Andreoni, W.; Curioni, A. *Appl. Phys. A* **1998**, *66*, 299.

(32) Ding, J.; Weng, L.-T.; Yang, S. *J. Phys. Chem.* **1996**, *100*, 11120.

(33) Lebedkin, S.; Renker, B.; Heid, R.; Schober, H.; Rietschel, H. *Appl. Phys. A* **1998**, *66*, 273.

(34) Weber, M. J.; Bierig, R. W. *Phys. Rev.* **1964**, *134*, 1492.

(35) Sato, N.; Mori, H.; Satoh, T.; Miura, T.; Takei, H. *J. Phys. Soc. Jpn.* **1988**, *57*, 1384.

(36) Yamada, M.; Kato, H.; Yamamoto, H.; Nakagawa, Y. *Phys. Rev. B* **1988**, *38*, 620.

(37) Terashima, T.; Kojima, N. *J. Phys. Soc. Jpn.* **1992**, *61*, 3303.